Partial Differential Equations in Applied Mathematics 10 (2024) 100659

Contents lists available at ScienceDirect

Partial Differential Equations in Applied Mathematics

journal homepage: www.elsevier.com/locate/padiff

Numerical study and optimization of a conical autoclave receiver

Khaled Mahdi [a,c,*], Khalida Bekrentchir [b], Nadir Bellel [c], Salah Boulaaras [d]

[a] Department of Physics, Faculty of Sciences, M'Sila University, PO Box 166 Ichebilia, M'Sila 28000, Algeria
[b] Department of Chemistry, Faculty of Sciences, M'Sila University, PO Box 166 Ichebilia, M'Sila 28000, Algeria
[c] Physics Energy Laboratory, Constantine 1 University, PO Box 325 Route de Ain El Bey, Constantine, Algeria
[d] Department of Mathematics, College of Science, Qassim University, Buraydah 51452, Saudi Arabia

ARTICLE INFO

Keywords:
Autoclave
Concentration ratio
Thermal efficiency
Saturated steam pressure
Thermal Energy

ABSTRACT

In this article, we present a mathematical model applied to the concentration of solar energy. This system is designed to prepare steam to meet the sterilization needs of medical instruments. A conical concentrator coupled to an autoclave in cylindrical form is placed in the conical reflector axis. We present a mathematical model explaining the thermal behaviour of water in a medical autoclave. The validation of the model was well done with the literature results. Our results indicate that the system produces saturated steam and takes 20 to 30 min, depending on climatic conditions and autoclave dimensions. The sufficient time to reach a temperature of more than 121 °C where no organism reproduces after being kept in an autoclave at 126 °C for 6 min or at 121 °C for at least 20 min. The simulation results encourage us to optimize the concentrator device to obtain a useful solar sterilizer, using the theoretical model as a safe guide to achieve this.

Introduction

Solar energy is one of the most important renewable energies we can rely on in the future. The continuous increase in population necessarily leads to a continuous increase in the consumption of energy, particularly fossil fuels, which, after being exploited, produce carbon dioxide, causing an increase in its percentage in the atmosphere and, therefore, an increase in greenhouse gas emissions. Which causes a climatic imbalance. Solar concentrators focus solar energy at high and medium temperatures for thermal or electricity generation applications. Depending on the type of concentration, solar concentrators can be classified as linear concentrators, such as a parabolic trough, or point concentrators, such as a solar parabolic dish. These two concentrators are a little difficult to produce because of their curvature, which requires fairly precise equipment. Conical concentrators are simple geometric shapes that are easy to create.[11718] The description of the solar autoclave includes a conical reflective surface, which we call a concentrator, and a cylindrical receiver (where we place the surgical instrument). This system must be equipped with a solar tracker to ensure maximum solar radiation reaches the system. The autoclave contains fluid such as water to ensure the thermal transfer of this concentrated energy to the medical equipment.[2,3] Exploiting solar energy using concentrators is interesting because it is affordable, accessible, and clean for the environment. Solar concentrator technology is simple and less expensive. For example, we can operate an autoclave without any cost, solving the problem of sterilizing medical instruments in developing countries and partially or isolated areas [15–17]. This work is presented in this thermodynamic study of the solar autoclave composed of a conical reflector and steam preparation system. To reproduce the system's transient behavior, we proposed an energy balance equation to carry out the model; this leads to a Partial differential equation for the temperature.[4] Solving the differential equation using the Runge-Kutta numerical method of order 4 gives us the temperature evolution of the autoclave and the water.[2] The temperature is an essential thermodynamic variable. With it, we have a clear idea of the time it will take for the autoclave to produce steam used for sterilization. To put the model into operation, we carried out several calculation tests. These simulations were carried out after we designed a system composed of a conical reflector and a cylindrical tube with a pressure regulator that contains water, which we call the autoclave. The tracking system was designed to make it easier for the reflector to recover as much radiation as possible to make the system efficient. The data obtained during the simulations are compared to the results in the literature. We find an excellent agreement between the two. The data obtained during the simulations are compared to the results in the literature. We find an excellent agreement between the two. The work is organized as follows: in the first section, we used Brichambaut model[5,6]

* Corresponding author at: Department of Physics, Faculty of Sciences, M'Sila University, PO Box 166 Ichebilia, M'Sila 28000, Algeria.
E-mail address: khaled.mahdi@univ-msila.dz (K. Mahdi).

https://doi.org/10.1016/j.padiff.2024.100659
Received 30 January 2024; Received in revised form 29 February 2024; Accepted 1 March 2024
Available online 12 March 2024

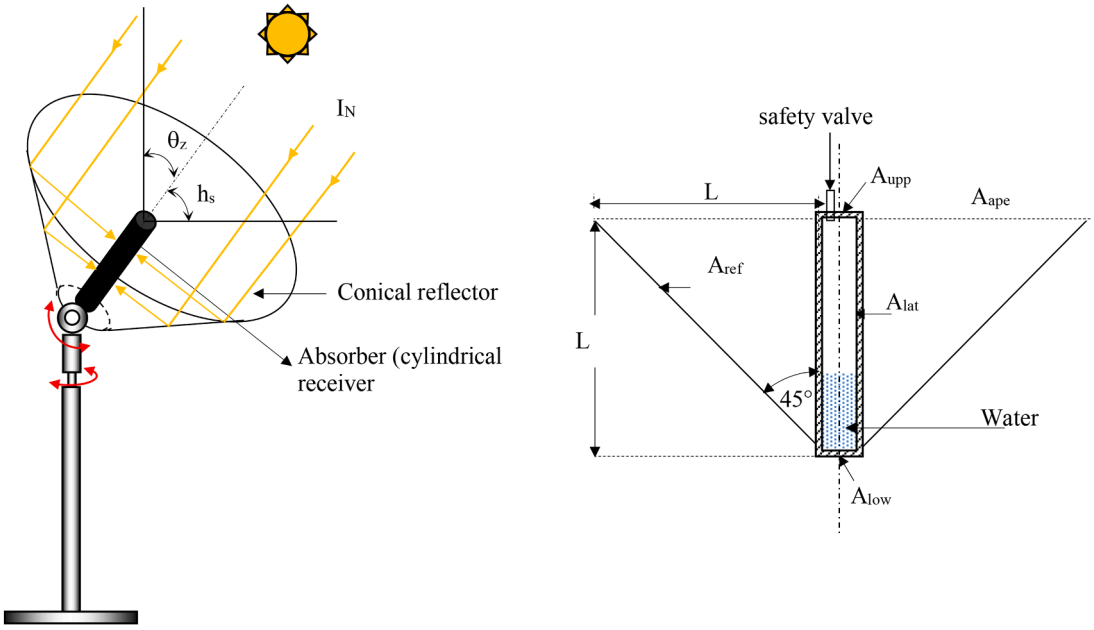

Fig. 1. Schematic of solar autoclave configuration.

to calculate the direct solar radiation at the M'Sila site; in the second section, we present the mathematical model developed to obtain the evolution of the temperature of the autoclave and water as well as the saturated steam pressure produced. Then, in Section 3, we present the designed device's performances and the comparison of the results with the seasons. Finally, in Section 4, we give our conclusions.

Description of the design

The concentrator is composed of a conical shape covered by a reflective material covering the reflector's interior surface. The conical concentrator/reflector rests on a support equipped with two axes of rotation following the sun. The metal of the autoclave must have good conductivity, so we chose copper (360 W/ °C.m^2) as the absorbent device. The autoclave is a tube with an external diameter of 5, 6, 7, 8, 9, and 10 cm and a length of 50 cm. It has a hole for filling with water (capacity according to the proposed diameter) and closes with a safety valve. The autoclave is covered with a thin layer of black paint to reduce the reflection of the sun's rays concentrated by the conical reflector. It is located in the conical concentrator axis. The half-angle of the top of the cone is 45° Fig. 1 shows a model proposed by.[5]

Where:

A_{ref}: reflector surface of the conical concentrator,
A_{ape}: aperture surface
A_{lat}: lateral surface of autoclave
A_{upp}: upper surface of the autoclave
Al_{ow}: lower surface of the autoclave
L: length of the autoclave/cylinder and radius of the aperture reflector
θ_z: zenith angle
h_s: solar height

Mathematical model

The mathematical model is composed mainly of two parts; the first calculates the direct incident radiation using solar radiation models.[1] The second is based on calculating the temperature and heat transfer parameters by convection, radiation, and saturated pressure[6] applied to the conical reflector and the absorber/autoclave.

Calculation of normal direct solar radiation

The solar autoclave was theoretically tested under M'Sila climatic conditions for the 21 December and 21 June, where computing started at 11:00 a.m. to 01:00 p.m. M'Sila is situated on a plateau at 340 m above sea level in the centre of Algeria (latitude 35.71° N, longitude 4.54° E). The region's climate is continental, characterized by Brichaumbot model.[6] Direct solar radiation can penetrate the atmosphere, but its intensity is attenuated. Various methods are used to calculate this radiation: the declination value can be obtained accurately using the following formula.[1]

$$\delta = 23.45\ sin\left[\frac{360}{365}\left(284 + n_{day}\right)\right] \tag{1}$$

With n_{day}: number of the day of the year (1st January $\equiv$ 1), declination is greatest at the summer solstice (21 June) and least at the winter solstice (21 December). it is zero at the equinoxes (21 March and 21 September). The position of the sun in the sky gives us information about solar time ST, which is given by sundials. There is a simple relationship between solar time ST and the hour angle w, given by:

$$\omega = (ST - 12) \times\ 15 \tag{2}$$

The notion of average time (STM), which varies by ±16 min about ST, is given by the following formula:

$$STM = ST - ET \tag{3}$$

Where the corrective term Et is called the equation of time, this quantity can be calculated using the following formula:

$$Et = 229.2(0.000075 + 0.001868\ \times cosB - 0.032077\ \times sinB - 0.014615 \times cos2B - 0.04089\ \times sin2B) \tag{4}$$

Where: $B = (n_{day} - 1)\frac{360}{365}$

The zenith angle θz, slope angle, hour angle, and azimuth angle are also calculated using formulas mentioned in the following equation:

$$\theta_z = \text{acos}(\cos(lat) \times \cos(\delta) \times \cos(\omega) + \sin(lat) \times sin(\delta)) \tag{5}$$

The following formula can be used to calculate the solar height:

$$h_s = asin[cos(lat) \times cos(\delta) \times cos(\omega) + sin(lat) \times sin(\delta)] \quad (6)$$

Direct solar radiation manages to pass through the atmosphere but suffers a reduction in its intensity. The calculation of this radiation follows different methods among this method:

The atmospheric pressure as a function of the altitude of the local point[7]

$$P_{atm} = 101325 \times \left(1 - z \times 2.26 \times 10^{-5}\right)^{5.26} \quad (7)$$

where:

z: Altitude in meters

The saturation vapour pressure P_{vs},[7] the average relative humidity U and the partial pressure of water vapour P_{vs} are defined by the following relationship

$$P_{vs} = 2.165 \times \left(1.098 + T_{env} \times 10^{-2}\right)^{8.02} \quad (8)$$

and

$$P_v = P_{vs} \times U \quad (9)$$

where:

U:relative humidity measured as a percentage (%)
T_{env}: Air temperature in °C.

The relative optical air mass m from which results the Rayleigh optical thickness E_R which determines the attenuation due to diffusion, the solution of Eq. (10) was made by Kasten[7]

$$m = \frac{P_{atm,}}{\left[101, 325,\ si, n\left(, h_{s,}\right) +, 151, 98., 75\ , \times\left(, 3.8, 85 +, h_{,s}\right), ^{-1.25,3}\right]} \quad (10)$$

and

$$E_R = \frac{1}{(0.9\ \times m + 9.4)} \quad (11)$$

Where:

E_R: Rayleigh optical thickness

In the Link method, we introduce the total cloudiness factor T_L, defined as the pure and dry atmospheric number (without aerosol, water vapour or cloud), that is to say, the manifestation only absorption and diffusion of the constituents of the atmosphere (O_2, CO_2, rare gases, etc.) The Linke T_L disorder factor allows an evaluation of atmospheric extinction by gases and aerosols according to the following formula[8]:

$$T_L = 2.4 + 14.6 \times d + 0.4 \times (1 + 2 \times d) \times \ln(P_v) \quad (12)$$

Where d is the coefficient of atmospheric disorder, which takes the values of:

d: 0.02 for a mountain location;
d: 0.05 for a rural location;
d: 0.10 for an urban location;
d: 0.20 for an industrial location (polluted atmosphere).

The calculation of extraterrestrial radiation can be carried out by the following approximate formula[1–9]:

$$G_{on} = G_{sc}\left[1 + 0.033\ cos\left(\frac{360}{3650} n_{day}\right)\right] \quad (13)$$

The calculation of incident radiation using the following formula:

$$I_N = G_{on} \times e^{-(E_R \times m \times T_L)} \quad (14)$$

The radiation flux concentrated on the lateral surface of the autoclave as shown in Fig. 1 by the following formula[2,3]:

$$Q_{aut} = I_N A_{ape} \rho_{ref} \alpha_{aut} \quad (15)$$

Mathematical description of the solar autoclave

In this paragraph, in Fig. 3, we observe that the concentration ratio for a parabolic dish concentrator can deliver theoretical concentrations higher by 100 to 10,000, which is enormous. In practice, conical concentrators are produced whose achievable concentration ratios are much smaller than 100, taking into account the contribution of optical errors on the geometric quality of the surfaces, the sun tracking error and the sun tracking and specular error. Focus. From the receptor, concentrations of around ten can be obtained. The main mathematical equations to describe the problem are presented. Eq. (16) determines the concentration ratio of the cone reflector.[1]

$$C_R = \frac{A_{apr}}{A_{lat}} \quad (16)$$

This equation is the ratio between the reflector's conical opening and the autoclave's side surface—the concentration ratio classification according to the reflector's geometric shape, according to Fig. 3. The present study chooses several different diameters (D_{aut} = 0.025, 0.03, 0.035, 0.04, 0.045, 0.05 m) of the autoclave for the same diameter of reflector D_{ref} = 1 m., which produces several different concentration ratios.

Energy balance of an autoclave

In this first part of the description of the solar autoclave, we have selected the mathematical model of the water heating system to produce saturated steam to sterilize medical-surgical instruments. The model comes from an energy balance carried out on the thermodynamic system we have defined (Fig. 1). The autoclave system is composed of the water in the lower part of the cylinder, which gives shape to the autoclave. Under these assumptions, the general energy balance is given by:

$$Q_{aut} = Q_{use} + Q_{los} \quad (17)$$

The energy concentrated by the conical reflector is provided by solar radiation. The amount of energy that the concentrator can supply to the autoclave system is:

$$Q_{aut} = \eta_O Q_s \quad (18)$$

Knowing that:

$$\eta_O = \rho_{ref}\ \alpha_{lat}$$

Where

$\alpha_{aut} = \alpha_{lat} = \alpha_{upp}$: Absorption coefficient, respectively, of the side and upper surface of the autoclave.

The following equation expresses the concentrated radiation provided by the conical concentrator/reflector:

$$Q_s = I_N A_{ref}$$

The useful heat produced can be calculated as follows from the energy balance of the autoclave. The absorbed solar energy by autoclave Q_{aut} is separated into useful heat (Q_{use}) and thermal losses Q_{los} the absorbed power (Q_{abs}) is calculated from the solar power (Q_s) and the optical efficiency (η_O):

$$\eta_O = \rho_{ref}\ \alpha_{aut}$$

Moreover, in steady state, thermal losses (Q_{los}) can be separated into three categories: heat losses by radiation (Q_{rad}), heat losses by internal

convection (Q_{conv}):

$$Q_{los} = Q_{rad} + Q_{conv} \tag{19}$$

Internal convection thermal losses

Then convection heat losses are given by

$$Q_{conv} = h_{lat}A_{lat}(T_{lat} - T_{env}) + h_{upp}A_{upp}(T_{upp} - T_{env}) \tag{20}$$

The values of the heat transfer coefficients of the lateral surface h_{lat} are highly dependent on the velocity of the wind blowing with respect to the cylinder. The heat transfer coefficient h_{lat} is given by.[1,2]

$$h_{lat} = 0.174\frac{\lambda_{aut}}{D}\left(\frac{\rho_{air}V_{wind}cosh_sD}{\mu_{air}}\right)^{0.618} \tag{21}$$

Where

λ_{aut}: Thermal conductivity of autoclave.
D: external diameter of autoclave.
ρ_{air}: Volumic mass of air
μ_{air}: dynamic viscosity of air

We can also calculate the Nusselt number using the following formula.

$$Nu_{lat} = \frac{h_{lat}D}{\lambda_{aut}} \tag{22}$$

and

$$Nu_{lat} = 0.174\left(\frac{\rho_{air}V_{wind}cosh_sD}{\mu_{air}}\right)^{0.618} \tag{23}$$

Where:

Nu_{lat}: Nusselt number of the autoclave lateral surface

The coefficient of the upper surface h_{lat}, when the wind speed is zero, is given by[10]

$$h_{lat} = \frac{k}{D^*}(Gr \times Pr \times cos\ h_s)^{0.25} \tag{24}$$

with

$$Nu_{lat} = (Gr \times Pr \times cos\ h_s)^{0.25} \tag{25}$$

where:

Gr:Grashof number,
Pr: Prandtl number.and

$$D^* = \sqrt{\pi\frac{D^2}{4}} \tag{26}$$

where

D*: dimensions of the side of a square whose area is equal to surfacewe can find the value of Grashof number by the relation

$$Gr = \frac{gy\Delta TL^3\rho^2}{\mu^2} \tag{27}$$

and

$$Pr = \frac{\mu c_p}{k} \tag{28}$$

where:

$$\Delta T = T_{aut} - T_{ref}$$

Radiation thermal losses

Then radiation heat losses are given by

$$Q_{rad-lat} = \frac{A_{lat}\varepsilon_{lat}}{1-\varepsilon_{lat}}\left(\sigma T_{lat}^4 - J_{lat}\right) + \frac{A_{upp}\varepsilon_{upp}}{1-\varepsilon_{upp}}\left(\sigma T_{upp}^4 - J_{upp}\right) \tag{29}$$

Where the radiosities J_{lat} and J_{upp} are developed in the appendix,[10,11] and are given by:

$$J_{lat} = \varepsilon_1\sigma T_{lat}^4 + (1-\varepsilon_{lat})\left(\varepsilon_{ref}F_{lat-ref} + \varepsilon_aF_{lat-ape}\right)\sigma T_{env}^4 \tag{30}$$

$$J_{upp} = \varepsilon_2\sigma T_{upp}^4 + \left(1-\varepsilon_{upp}\right)\left(\varepsilon_gF_{upp-g}\sigma T_g^4 + \varepsilon_aF_{upp-s}\sigma T_{env}^4\right) \tag{31}$$

where:

ε_{lat}: emissivities of the lateral surface of the autoclave
ε_{ref}: emissivities of the conical surface of the concentrator/reflector
ε_{upp}: emissivities of upper surface of the autoclave

The radiosities J_{lat}, J_{upp} and J_{ref}, are calculated by following equations[5]

$$J_{lat} = \varepsilon_{lat}\sigma T_{lat}^4 + (1-\varepsilon_{lat})\left(J_{ref}F_{lat-ref} + J_{ape}F_{lat-ape}\right) \tag{32}$$

$$J_{ref} = \varepsilon_{ref}\sigma T_{ref}^4 + \left(1-\varepsilon_{ref}\right)\left(J_{lat}F_{ref-lat} + J_{ref}F_{ref-ref} + J_{lat}F_{ref-lat}\right) \tag{33}$$

$$J_{ape} = \varepsilon_{ref}\sigma T_{ref}^4 + 0 = \varepsilon_{env}\sigma T_{env}^4 \tag{34}$$

and

$$F_{lat-ape} = \frac{1}{2\pi}\left(cos^{-1}\frac{B}{A} - \frac{1}{2y}\left[\sqrt{\left((A+2)^2 - 4x^2\right)}\,cos^{-1}\frac{B}{xA} + Bsin^{-1}\frac{1}{x} - \frac{\pi A}{2}\right]\right) \tag{35}$$

Where

$$x = \frac{R_{ape}}{R_{aut}} \tag{36}$$

We can also calculate the ratio

$$y = \frac{L}{R_{aut}} \tag{37}$$

With:

L: length of the autoclave
R_{ape}: radius of the conical aperture
R_{aut}: radius of the autoclaveand

$$A = x^2 + y^2 - 1 \tag{38}$$

$$B = y^2 - x^2 + 1 \tag{39}$$

Since surface two is always kept normal to the solar rays, then:

$$F_{upp-gro} = \frac{1}{2}[1 - \sin(h_s)] \tag{40}$$

$$F_{upp-sky} = \frac{1}{2}[1 + \sin(h_s)] \tag{41}$$

Where:

$F_{uoo\text{-}gro}$: shape factor of the upper surface of the autoclave to the ground
$F_{uoo\text{-}gro}$: shape factor of the upper surface of the autoclave to the sky

The emissivity ε_a of the atmospheric air is given by,[11,12]

$$\varepsilon_a = 1 - 0.261\ e^{\left[-7.77\ \times 10^{-4}T_{env}^2\right]} \tag{42}$$

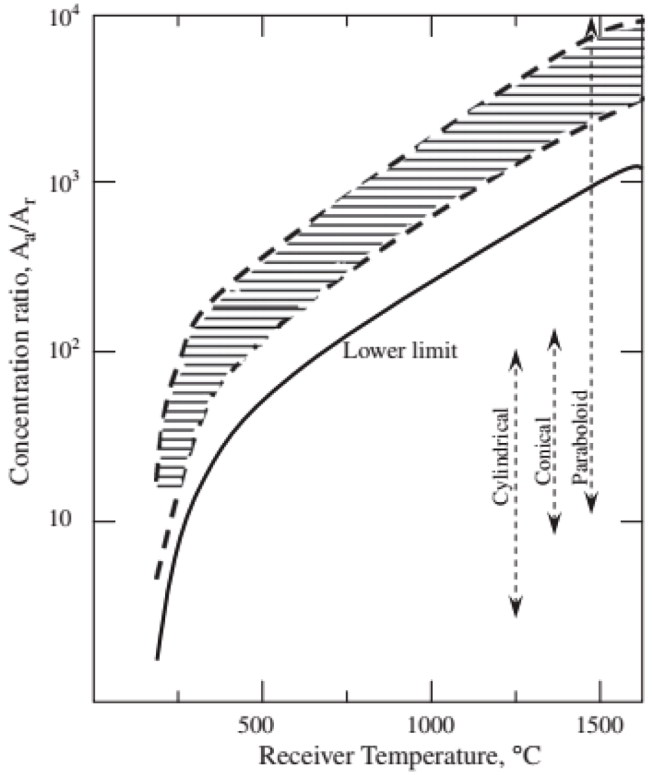

Fig. 2. Curves of concentration ratio C_R as a function of receiver temperature for different geometric shapes of reflector.[1]

$$(m_{water}c_{water} + m_{aut}c_{aut})\frac{dT_{aut}(t)}{dt} = I_N A_{ape}\rho_{ref}\alpha_{lat} - \Big[h_{lat}A_{lat}(T_{lat} - T_{env}) + h_{upp}A_{upp}(T_{upp} - T_{env}) + \frac{A_{lat}\varepsilon_{lat}}{1-\varepsilon_{lat}}(\sigma T_{lat}^4 - J_{lat}) + \frac{A_{upp}\varepsilon_{upp}}{1-\varepsilon_{upp}}(\sigma T_{upp}^4 - J_{upp})\Big] \quad (43)$$

Where:

σ: Stefan-Boltzmann constant, 5.67×10^{-8} W/m^{2}K^4
m_{water}: mass of the water in the autoclave
m_{aut}: mass of the autoclave.

the value of T_{aut} being obtained by solving the equation by a numerical method (Range-Kutta of order 4). the autoclave fluid temperature defined as:

$$T_{water} = \frac{T_{aut} + T_{env}}{2} \quad (44)$$

Thermal efficiency of the solar autoclave

The thermal efficiencies for different receiver tube diameters and different inlet temperatures are calculated and plotted in Fig. 11. The following expression gives the thermal efficiency of such a device[13]:

$$\eta_{th} = F_R\eta_O - \left(\frac{F_R U_L}{C_R}\right)\frac{T_{lat} - T_{env}}{I_N} \quad (45)$$

$$\eta_O = \rho_{ref}\alpha_{lat} = 0.9 \times 0.95 = 85\%$$

where F_R: heat removal factor[5] is given by:

$$F_R = \frac{m\ c_{water}}{A_{lat}U_L}\left[1 - exp\left(-\frac{A_{lat}U_L F'}{\dot{m}c_{water}}\right)\right] \quad (46)$$

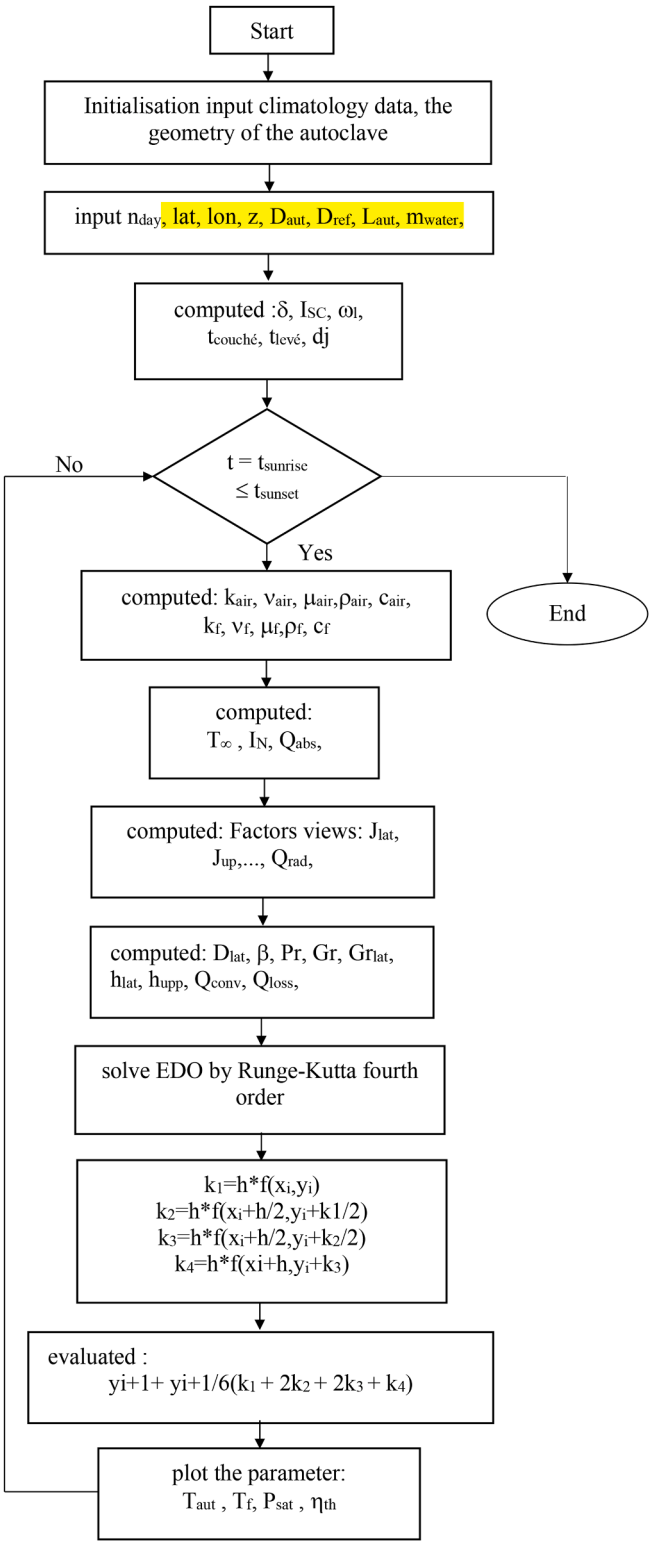

Fig. 3. Flowchart for calculating physical parameters.

where:

F': collector efficiency factor
U_L: overall heat loss coefficient from autoclave
m: masse of the water

To determine the heat loss coefficient U_L, we can use Eq. (47).

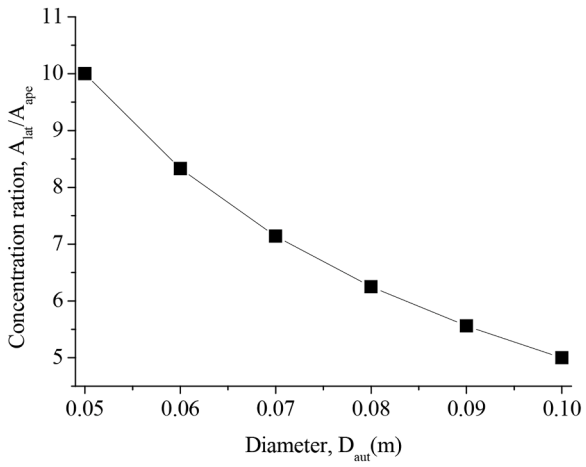

Fig. 4. variation of concentration ratio with variation of autoclave diameter.

$$U_L = \frac{Q_{los}}{A_{aut}(T_{aut} - T_{mv})} \tag{47}$$

Clapeyron 's equation gives the evolution of the pressure of the saturated steam of the water in the autoclave as a function of the change in its temperature is given by[11]:

$$p_{sat} = p_0 exp\left[\frac{M.L_v}{R}(1/T_O - 1/T_{water})\right] \tag{48}$$

Where:

T_O: boiling temperature of the water at a given pressure p_0, in K;
p_{sat}: saturated vapor pressure, in the same unit as p_0;
M: molar mass of the water, in kg/mol, for water $M = 0.018$ kg/mol;
L_v: latent heat of vaporization of the substance, in J/kg, $L_v = 2.26 \times 10^6$ J/kg (at 100 °C);
R: ideal gas constant, equal to 8.31 J mol^{-1} K^{-1};
T: steam temperature, in K.

Computer program for simulation

We have developed a computational code in Fortran language, which can provide early knowledge about temperature distribution, solar irradiation and temperature at the receiver/autoclave. The Runge-Kutta algorithm of order 4 allows the solution of the partial differential equation. Fig. 2 and Fig. 3 shows the following flowchart, which presents the procedure for calculating the evolution of the temperature of the autoclave and what it contains, as well as the saturating pressure produced by heating the water.

Results and interpretations

In this part, the modelling results are presented. In all cases, the fluid's initial temperature and the environment were defined, and other parameters according to winter and summer, such as heating temperature, average autoclave temperature and thermal losses, were calculated. Fig. 4 shows that the concentration ratio decreases as the diameter

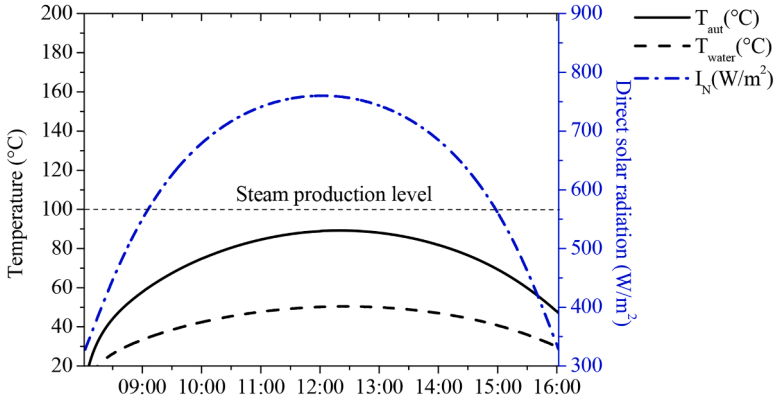

Fig. 5. Hourly variation of autoclave temperature (T_{aut}), ambient temperature (T_{env}) and direct normal solar radiation (I_N) for 21 December ($m = 0.9$ kg, $D_{aut} = 0.10$ m).

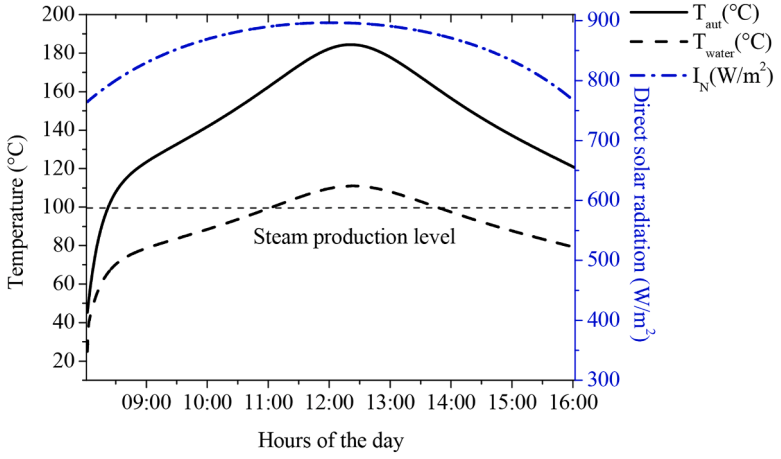

Fig. 6. Hourly variation of autoclave temperature (T_{aut}), ambient temperature (T_{env}) and direct normal solar radiation (I_N) for 21 June ($m = 0.9$ kg, $D_{aut} = 0.10$ m).

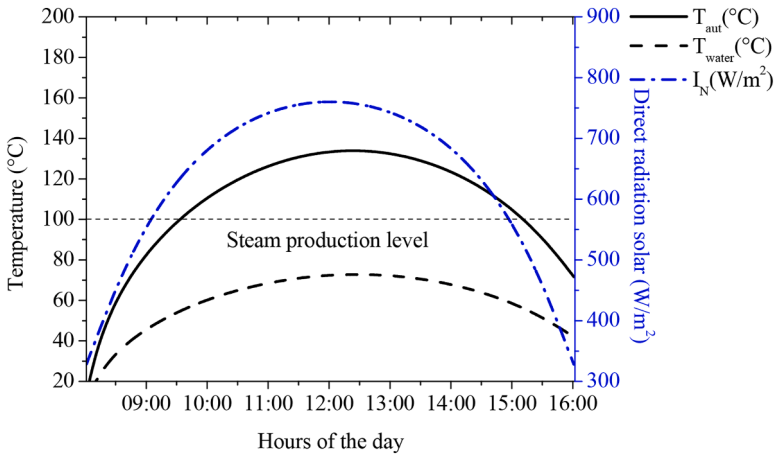

Fig. 7. Hourly variation of autoclave temperature (T_{env}), ambient temperature (T_{aut}) and direct normal solar radiation (I_N) for 21 December (m = 0.9 kg, D_{aut} = 0.05 m).

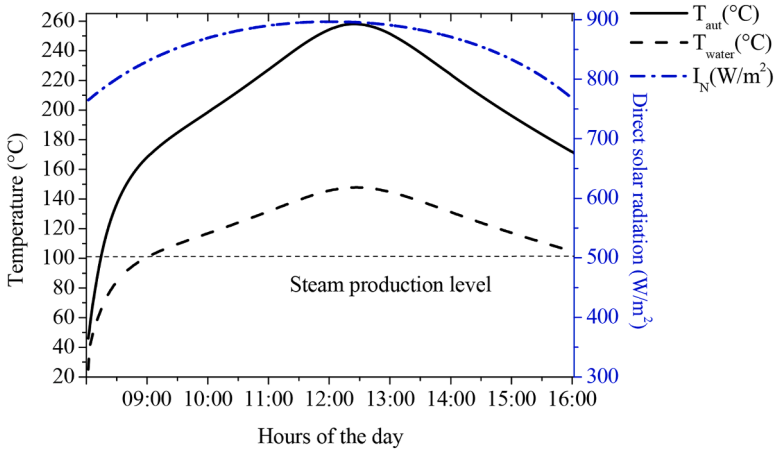

Fig. 8. Hourly variation of autoclave temperature (T_{env}), ambient temperature (T_{aut}) and direct normal solar radiation (I_N) for 21 June (m = 0.9 kg, D_{aut} = 0.05 m).

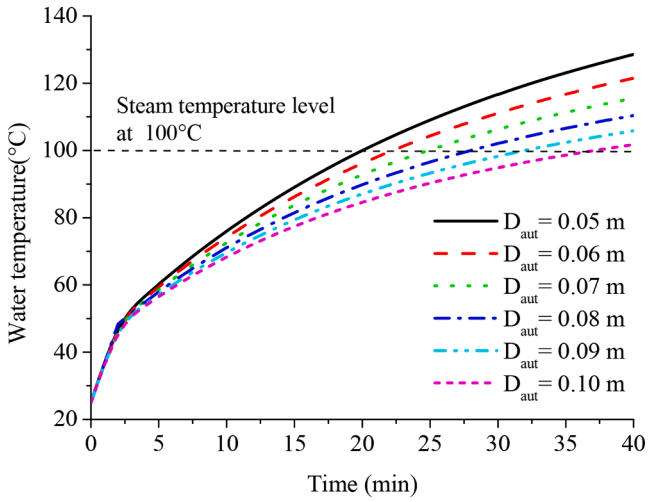

Fig. 9. Influence of the autoclave diameter.

of the conical concentrator autoclave increases[12].

The following Fig. 9 shows the influence of the diameter of the autoclave on the water temperature; the reduction in the diameter of the autoclave causes an increase in the geometric concentration, which therefore increases the temperature at the autoclave level. A sizeable geometric concentration, therefore, a large concentrated flow on the side surface of the autoclave increases the temperature value to high levels.[13]

This modelling approach was validated by comparing the mathematical model and Bahadori's numerical results (1976). The temperature distribution of the autoclave in March is compared with data measured by Bahdori (1976), as shown in Fig. 10. A good agreement is obtained between the numerical and measured data. The results are statistically significant, with a very high R square value (greater than 0.980) and a meager P value.

In Fig. 10, we observe the increase in wind speed, which will increase heat losses and thus reduce the temperature of the autoclave. The use of the solar autoclave for water heating and the production of saturated steam with a stationary fluid at the level of the autoclave is not very interesting because of the stagnation temperature reached after a very short time in the summer and relatively in the winter. The efficiency of the conical concentrator becomes zero after a specific heating time; it is necessary to change the contents of the autoclave, which allows us to conclude that this type of model cannot be used continuously all day.

We can define the stagnation temperature when the thermal efficiency of the autoclave equals zero. According to Eq. (49):

$$T_{stag} = \frac{C_R \rho_{ref}\ \alpha_{lat} I_N}{U_L} + T_{env} \tag{49}$$

The parameter presented is the thermal efficiency of the solar

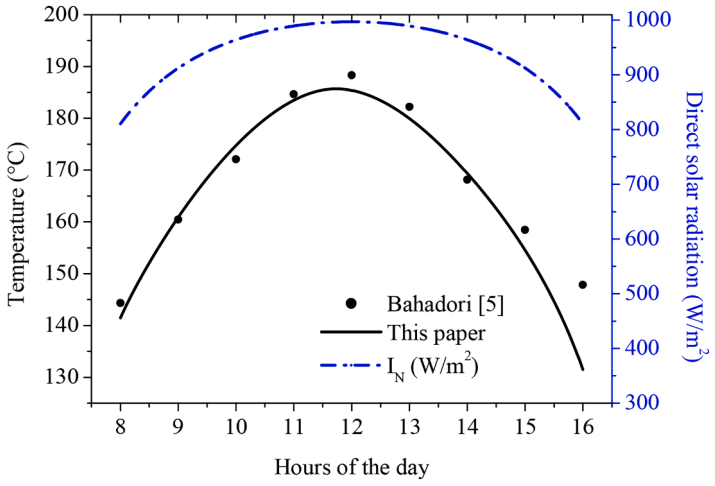

Fig. 10. Comparison of mathematical model results and Bahadori's data(1976 = 0.9 kg, D_{aut} = 0.05 m) for 21 June.

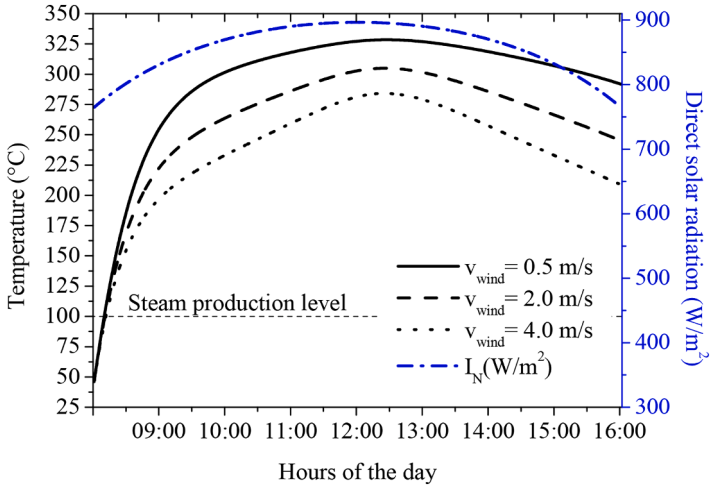

Fig. 11. Influence of wind on autoclave temperature for 21 June (m = 0.9 kg, D_{aut} = 0.05 m).

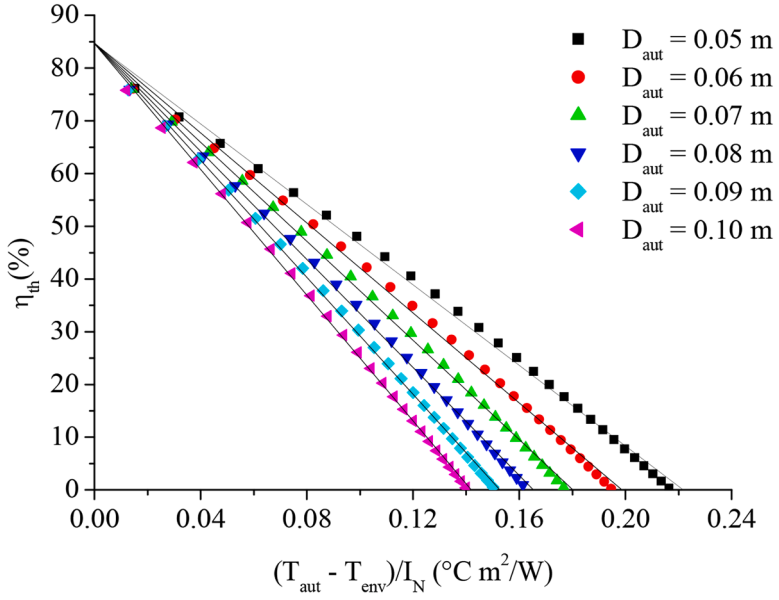

Fig. 12. Thermal efficiency curve for different diameters of the solar autoclave (mwater=0.3 kg).

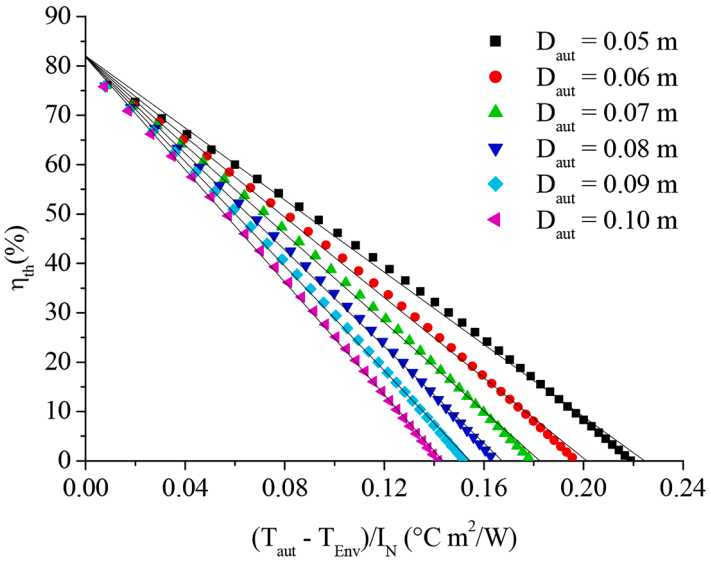

Fig. 13. Thermal efficiency curve for different diameter of the solar autoclave (m_{water}=0.6 kg).

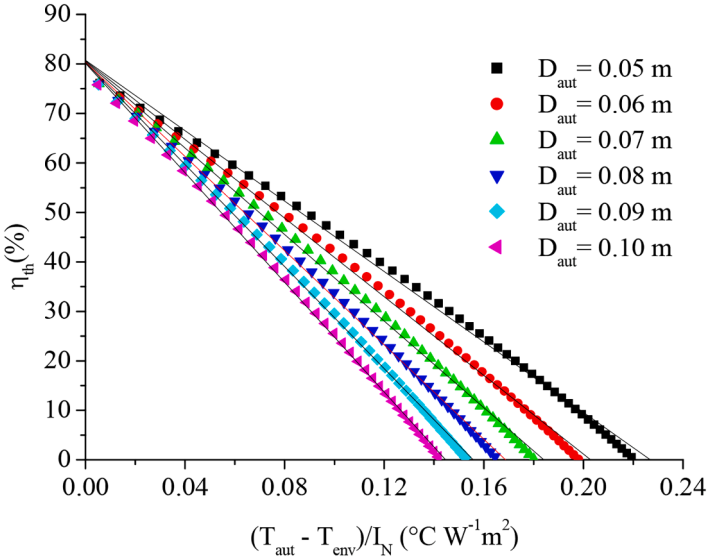

Fig. 14. Thermal efficiency curve for different diameter of the solar autoclave (m_{water}=0.9 kg).

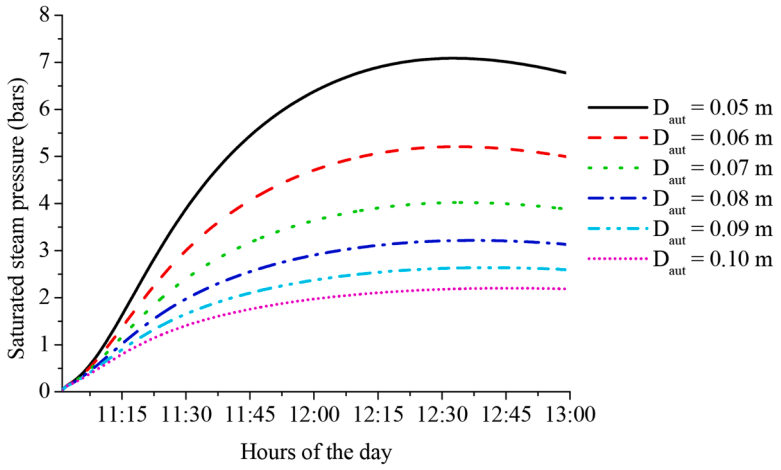

Fig. 15. variation de la pression en fonction de diamètre pour m = 0.3 kg for 21 June.

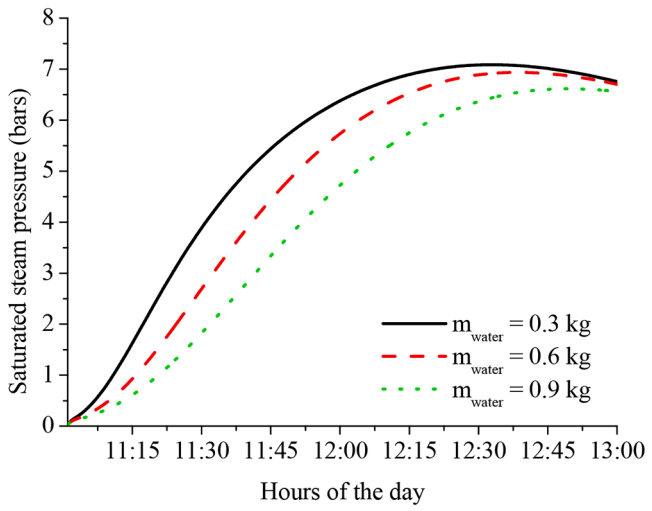

Fig. 16. variation de la pression en fonction de masse d'eau pour $D_{aut} = 0.05$ m for 21 June.

autoclave. Fig. 3 presents this quantity for different operating conditions. The x-axis is the efficiency parameter $(T_{aut} - T_{env})/I_N$, generally used to present the system efficiency. In the following three Figs., 11, 12 and 13, we have taken three different quantities of water in the autoclave $m_{water} = 0.3$, 0.6 and 0.9 kg for their same diameters.[14–17]

Equations that describe the thermal efficiency of the solar autoclave for different diameters are given as follows:

$$\text{For } D_{aut} = 0.05\text{m}: \ \eta_{th}(\%) = 84.6 - 3.816\left(\frac{T_{aut} - T_{env}}{I_N}\right)$$

$$\text{For } D_{aut} = 0.06\text{m}: \ \eta_{th}(\%) = 84.7 - 4.265\left(\frac{T_{aut} - T_{env}}{I_N}\right)$$

$$\text{For } D_{aut} = 0.07\text{m}: \ \eta_{th}(\%) = 84.7 - 4.698\left(\frac{T_{aut} - T_{env}}{I_N}\right)$$

$$\text{For } D_{aut} = 0.08\text{m}: \ \eta_{th}(\%) = 84.6 - 5.119\left(\frac{T_{aut} - T_{env}}{I_N}\right)$$

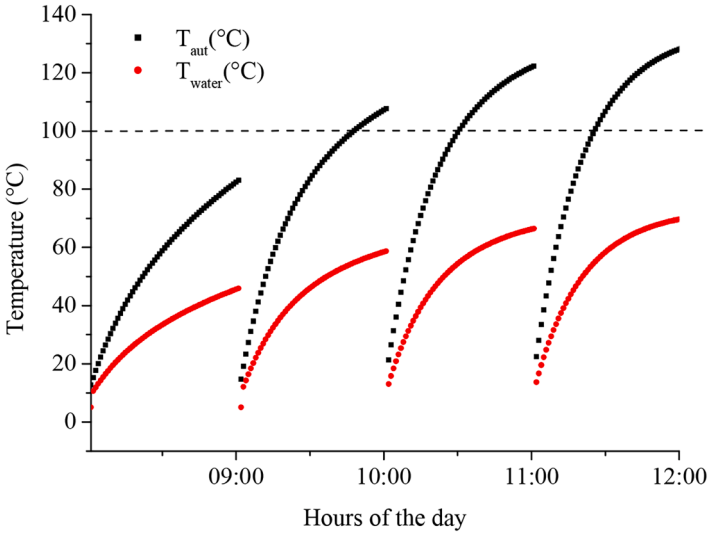

Fig. 17. Duration of heating of the autoclave water during the different hours of the day of December 21.

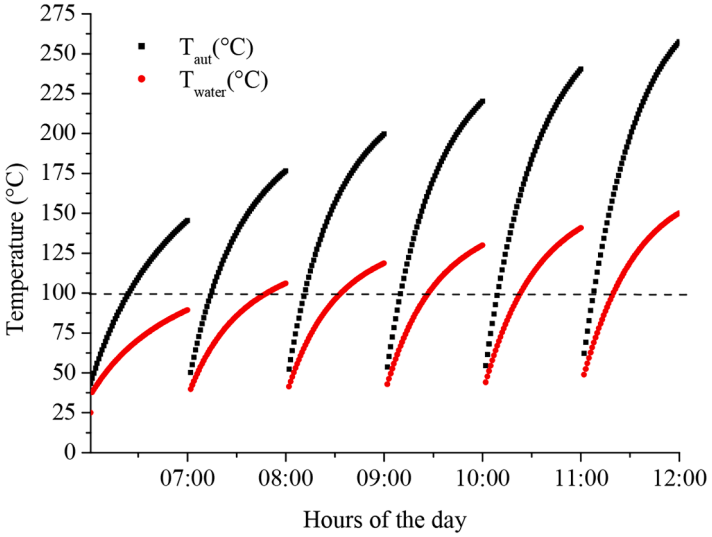

Fig. 18. Duration of heating of the autoclave water during the different hours of the day of June 21.

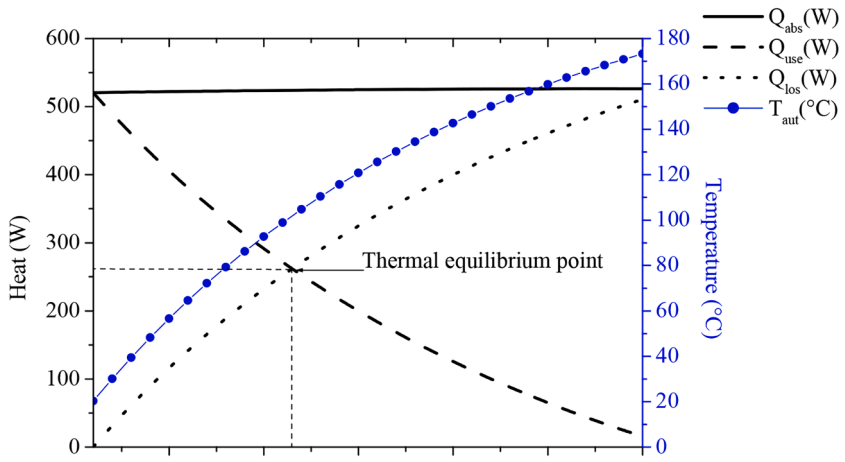

Fig. 19. Graph of simulation that began at 11:00 h solar time for 21 December, $\bar{I}_N$= 878.6 W/m^2, D_{aut} = 0.05 m, C_R ≈10, m_{water}= 0.6 kg.

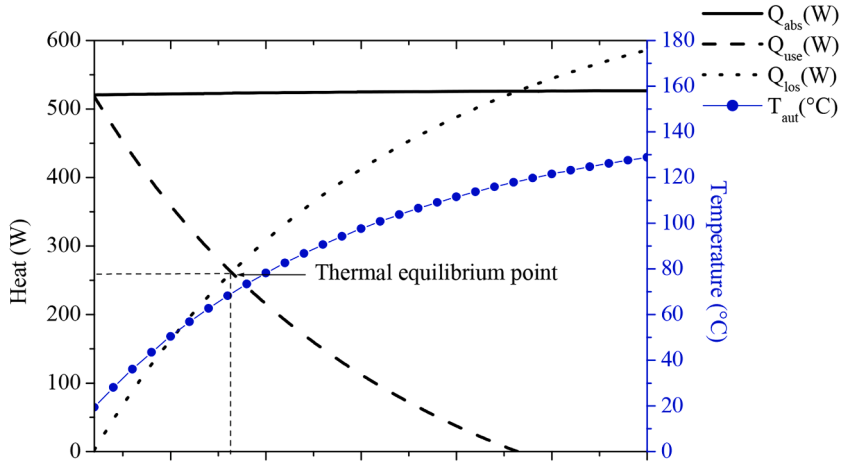

Fig. 20. Graph of simulation that began at 11:00 h solar time for 21 December,$\bar{I}_N$= 878.6 W/m^2, D_{aut} = 0.1 m, C_R ≈5, m_{water}= 0.6 kg.

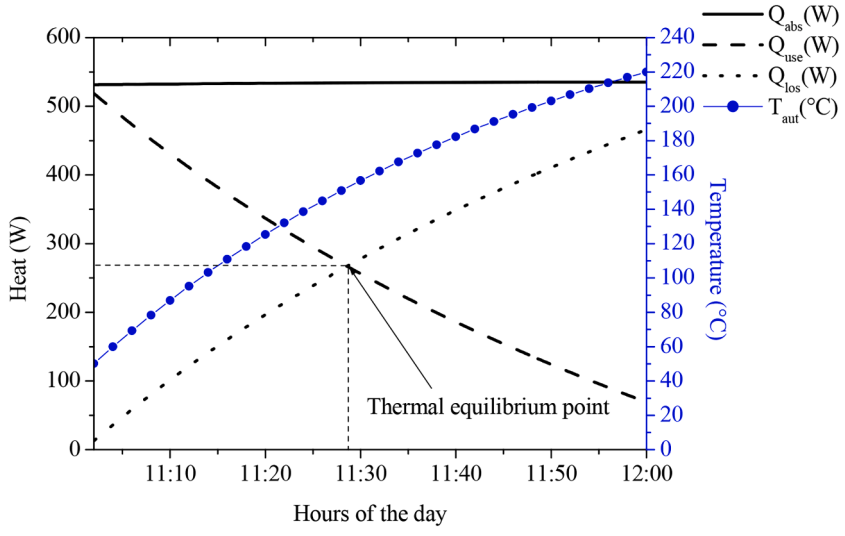

Fig. 21. Graph of simulation that began at 11:00 h solar time for 21 Jun, $\bar{I}_N$= 894.5 W/m^2, D_{aut} = 0.05 m, C_R ≈10, m_{water}= 0.6 kg.

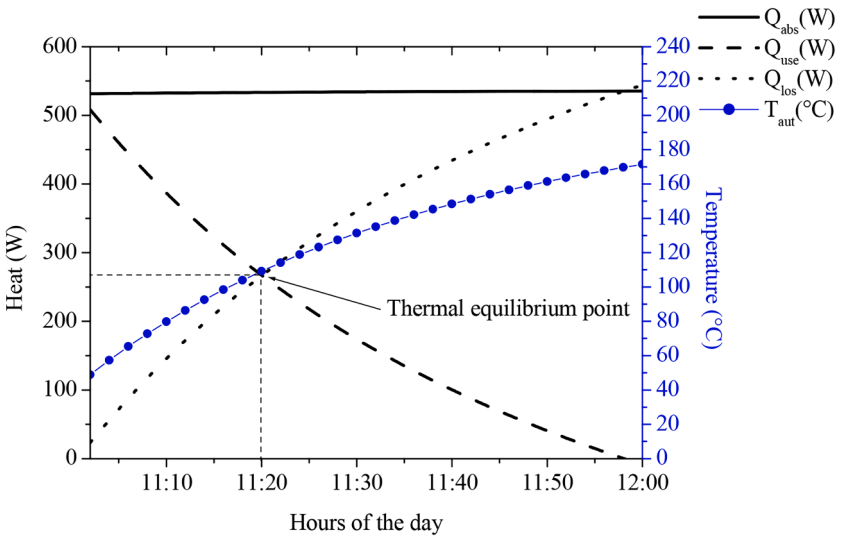

Fig. 22. Graph of simulation that began at 11:00 h solar time for 21 Jun, $\bar{I}_N$= 894.5 W/m^2, D_{aut} = 0.1 m, $C_R \approx 5$, m_{water}= 0.6 kg.

Table 1
Parameters of the investigated configurations.

Parameters	Symbol	Value
Lateral surface of the absorber	A_{lat} (m^2)	3.1415e−1
Upper surface of the autoclave	A_{upp}(m^2)	3.1415e−2
Lower surface of the autoclave	A_{low}(m^2)	3.1415e−2
Aperture surface of the cone	A_{apr} (m^2)	1.1309
Reflector surface of the cone	A_{ref} (m^2)	1.4721
Autoclave Length	L (m)	0.5
Concentration factor	C_R	A_{ape}/A_{lat}
Emissivity	ε_{lat}=ε_{upp}=ε_{ref}	0.95
Atmospheric emissivity	ε_{atm}	~ 0.7
Ground emissivity	ε_{gro}	0.9
reflector reflectivity	ρ_{ref}	0.8
Ground reflectivity	ρ_g	0.2

Table 2
Main results: F_R and U_L for different receiver tube diameters 0.3 kg.

coefficients	D = 0.05	0.06	0.07	0.08	0.09	0.10
C_R	10	8.33	7.14	6.25	5.56	5
$F_R\eta_O$	0.846	0.847	0.847	0.846	0.846	0.846
F_R	0.996	0.997	0.996	0.996	0.996	0.995
F_RU_L/C_R(%)	3.816	4.265	4.698	5.119	5.546	5.964
U_L(W/m^2 °C)	38.30	35.63	33.65	32.12	30.95	29.94
T_{stag} (°C)	239.3	219.6	203.3	189.4	179.1	169.9

Table 3
Main results: F_R and U_L for different receiver tube diameters 0.6 kg.

coefficients	D = 0.05	0.06	0.07	0.08	0.09	0.10
C_R	10	8.33	7.14	6.25	5.56	5
$F_R\eta_O$ (%)	82.063	81.931	81.888	81.822	81.839	81.801
F_R	0.965	0.963	0.963	0.962	0.962	0.962
F_RU_L/C_R(%)	3.654	4.070	4.485	4.889	5.299	5.698
U_L(W/m^2 °C)	37.85	35.18	33.24	31.74	30.60	29.60
T_{stag} (°C)	241.67	220.45	204.51	190.84	180.69	171.73

Table 4
Main results: F_R and U_L for different receiver tube diameters 0.9 kg.

coefficients	D = 0.05	0.06	0.07	0.08	0.09	0.10
C_R	10	8.33	7.14	6.25	5.56	5
$F_R\eta_O$(%)	80.766	80.651	80.52014	80.373	80.292	80.200
F_R	0.950	0.948	0.947	0.945	0.944	0.943
F_RU_L/C_R(%)	3.56	3.97	437.46	476.37	515.539	554.16
U_L(W/m^{2}K)	37.463	34.891	32.972	31.487	30.344	29.366
T_{stag} (°C)	241.97	222.64	206.42	192.39	181.51	171.83

$$\text{For } D_{aut} = 0.09\text{m}: \ \eta_{th}(\%) = 84.6 - 5.546\left(\frac{T_{aut} - T_{env}}{I_N}\right)$$

$$\text{For } D_{aut} = 0.10\text{m}: \ \eta_{th}(\%) = 84.6 - 5.964\left(\frac{T_{aut} - T_{env}}{I_N}\right)$$

Equations that describe the thermal efficiency of the solar autoclave for different diameters are given as follows:

$$\text{For } D_{aut} = 0.05\text{m}: \ \eta_{th}(\%) = 82.063 - 3.654\left(\frac{T_{aut} - T_{env}}{I_N}\right)$$

$$\text{For } D_{aut} = 0.06\text{m}: \ \eta_{th}(\%) = 81.931 - 4.070\left(\frac{T_{aut} - T_{env}}{I_N}\right)$$

$$\text{For } D_{aut} = 0.07\text{m}: \ \eta_{th}(\%) = 81.888 - 4.485\left(\frac{T_{aut} - T_{env}}{I_N}\right)$$

$$\text{For } D_{aut} = 0.08\text{m}: \ \eta_{th}(\%) = 81.822 - 4.889\left(\frac{T_{aut} - T_{env}}{I_N}\right)$$

$$\text{For } D_{aut} = 0.09\text{m}: \ \eta_{th}(\%) = 81.839 - 5.299\left(\frac{T_{aut} - T_{env}}{I_N}\right)$$

$$\text{For } D_{aut} = 0.10\text{m}: \ \eta_{th}(\%) = 81.801 - 5.698\left(\frac{T_{aut} - T_{env}}{I_N}\right)$$

Equations that describe the thermal efficiency of the solar autoclave for different diameters are given as follows:

$$\text{For } D_{aut} = 0.05\text{m}: \eta_{th}(\%) = 80.766 - 3.559\left(\frac{T_{aut} - T_{env}}{I_N}\right)$$

$$\text{For } D_{aut} = 0.06\text{m}: \ \eta_{th}(\%) = 81.931 - 4.070\left(\frac{T_{aut} - T_{env}}{I_N}\right)$$

$$\text{For } D_{aut} = \ 0.07\text{m}: \ \eta_{th}(\%) = 81.888 - 4.485\left(\frac{T_{aut} - T_{env}}{I_N}\right)$$

$$\text{For } D_{aut} = \ 0.08\text{m}: \ \eta_{th}(\%) = 81.822 - 4.889\left(\frac{T_{aut} - T_{env}}{I_N}\right)$$

$$\text{For } D_{aut} = \ 0.09\text{m}: \ \eta_{th}(\%) = 81.839 - 5.299\left(\frac{T_{aut} - T_{env}}{I_N}\right)$$

$$\text{For } D_{aut} = \ 0.10\text{m}: \ \eta_{th}(\%) = 81.801 - 5.698\left(\frac{T_{aut} - T_{env}}{I_N}\right)$$

This coefficient is relatively big because there is no coverage and convection losses are significant. The thermal convection coefficient is approximately 10 W/m^2 °C, so the total heat loss coefficient is greater than this value, varying from approximately 29.36 to 38.30 W/m^2 °C. These high values are acceptable because radiation losses are included. We noted that the thermal efficiency is maximum when the temperature of the autoclave is equal to the temperature of the environment.[14,17]

This situation only occurs at the start of each heating operation. The increase in temperature reduces the thermal efficiency of the autoclave. The efficiency of the autoclave decreases remarkably when the diameters of the autoclave increase because the autoclave transfers a large part of the heat to the external environment due to the increase in their lateral surface, which explains a decreased concentration ratio C_R. We also observe no variation in the shape of the curves when we change the quantity of water.

Fig. 15w shows the influence of the diameter of the autoclave on the pressure of the saturated steam; the increase in the diameter of the autoclave causes a reduction in pressure, which, therefore, reduces the temperature at the level of the autoclave. An increase in the geometric concentration, therefore, causes a concentrated flow to increase on the side surface of the autoclave, which will increase the temperature value to higher levels and cause an increase in the steam pressure[14]. We note in Fig. 16 that when we increase the mass of water added to the autoclave, we will increase steam production and pressure by a few more bars.

Figs. 17 and 18 show the variation in the temperature of the autoclave and the water during these two days (December 21 and June 21). Temperature increases over time in all operations. After each cooling, the temperature of the autoclave and the water becomes equal to the temperature of the environment. There is a difference between the autoclave temperature in winter and summer due to the power of solar radiation. We also notice that the heating speed in summer is more than three times more rapid compared to winter Figs. 8, 14.

In Figs. 19, 20, 21 and 22, we show the evolution of heat losses and the heat used and absorbed during heating on December 21 for two different diameters of the autoclave $D_{aut} = 0.05$ and 0.10 m. It can be seen that the heat absorbed by the side surface of the autoclave is lower than the heat received by the conical opening of the reflector. This variation is due to losses by reflection and absorption by the conical reflector and the autoclave Figs. 6, 7.

When the temperature of the side surface of the autoclave increases, the latter transfers heat to the environment by conduction, radiation and convection. The more significant the difference between the temperature of the absorber and the ambient air, the greater the heat losses from the conical concentrator and the lower the useful heat. Heating continues until reaching the point of thermal equilibrium between useful heat and waste heat, i.e. at 11:22 a.m. for $D_{aut} = 0.05$ m and 11:16 a.m. for $D_{aut} = 0.10$ m in winter and at 11:28 a.m. for $D_{aut} = 0.05$ m and 11:20 a.m. for $D_{aut} = 0.10$ m in summer.[2] At this point, the equilibrium temperature is reached (Fig. 2, 5–8,14 and Table 1–4).

Conclusion

This article presents a mathematical model for the evolution of the water temperature in an autoclave operating with solar energy supplied by a conical reflector. We have also validated the model with work published in the literature. Although the model is simple, it is capable of describing physical phenomena. It can accurately reproduce the phase change point within 100 °C when the phase transition begins in the thermodynamic system. The concentration ratio of the order of 10 can operate from the production of steam combined with relatively medium radiation. The time necessary to produce the saturating steam to reach pressures of around 7 bars. For a diameter of 0.05 m in normal conditions. The mathematical model effectively predicts the evolution of the temperature of the autoclave and the water. Thanks to it, we can propose modifications to the system, which will allow it to function more optimally.

Declaration of competing interest

The authors declare that they have no known competing financial interests or personal relationships that could have appeared to influence the work reported in this paper.

Data availability

No data was used for the research described in the article.

References

1. Duffie AJ, Backman WA. *Solar Engineering of Thermal Processes*. 2nd ed. New York: John Wiley; 1991. https://doi.org/10.1002/9781118671603.
2. Mahdi K, Bellel N. Development of a spherical solar collector with a cylindrical receiver. *Energy Procedia*. 2014;52:438–448. https://doi.org/10.1016/j.egypro.2014.07.096.
3. Mahdi K, Bellel N. Estimation of steam production in a receiver under solar concentrating radiation. *Contemp Eng Sci*. 2014;7:835–843. https://doi.org/10.12988/ces.2014.4652.
4. Bahadori MN. Design of a solar autoclave. *Sol Energy*. 1976;18:489–496. https://doi.org/10.1016/0038-092X(76)90068-2.
5. Mathur SS, Sharma JK, Dang A, Garg HP. Design and development of a solar conical concentrator. *Int J Energy Res*. 1982;6:73–81. https://doi.org/10.1002/er.4440060109.
6. Brichambaut, P.D., Vauge C. Le gisement solaire: évaluation de la ressource énergétique, Technique Et Documentation, 1982, Paris.
7. Mefti A, Bouroubi MY, Khellaf A. Analyse Critique du Modèle de l'Atlas Solaire De l'Algérie. *Rev Energy Ren*. 1999;2:69–85.
8. Bernard R, Menguy G, Schwartz M. *Le rayonnement solaire. Technique Et Documentation*. Paris: Lavoisier; 1979.
9. Rohsenow WM, Hartnett JP. *Radiant interchange between surfaces separated by non absorbing and non emitting media. Handbook of Heat Transfer*. New York: McGraw-Hill; 1973:15–29. to 15-52.
10. Capderou M. *Atlas Solaire De l'Algérie, Tome 1, vol1 Et 2, Modèles Théoriques Et Expérimentaux*. Algérie: Office des Publications Universitaires; 1987.
11. hofierka J, sùri M. the solar radiation model for open source GIS: implementation and applications. In: *Proceedings of the Open Source GIS-GRASS Users Conference*. 2002.
12. behar O, khellaf A, Mohammedi K. comparison of solar radiation models and their validation under algerian climate–the case of direct irradiance. *Energy Convers Manag*. 2015;(98):236–251.
13. Karlekar BV, Desmond RM. *Engineering Heat Transfer*. New York: West Publishing Co.; 1977:439–440.
14. Kreith F. *Principles of Heat Transfer*. New York: IEP-A Dun Donnelley publisher; 1976.
15. Steward WG, Kreith F. Stationary concentrating reflector cum tracking absorber solar energy collector: optical design characteristics. *Appl Opt*. 1975;14(7).
16. Faiman D., Solar thermal collectors. Introduction to solar energy. Lecture 5 version 3 .1, 2003.
17. Irkıl N, Mahdi K, Pişkin E, Alnegga M, Boulaaras S. On a logarithmic wave equation with nonlinear dynamical boundary conditions: local existence and blow-up. *J Inequal Appl*. 2023. https://doi.org/10.1186/s13660-023-03072-3.
18. Viessmann SA. Solaire L'énergie permet de réduire les coûts de chauffage. *Brochure Techn Sol*. 2003;09.